# Lab Notes

**Editors**
Thomas M. Moses | Shane F. McClure

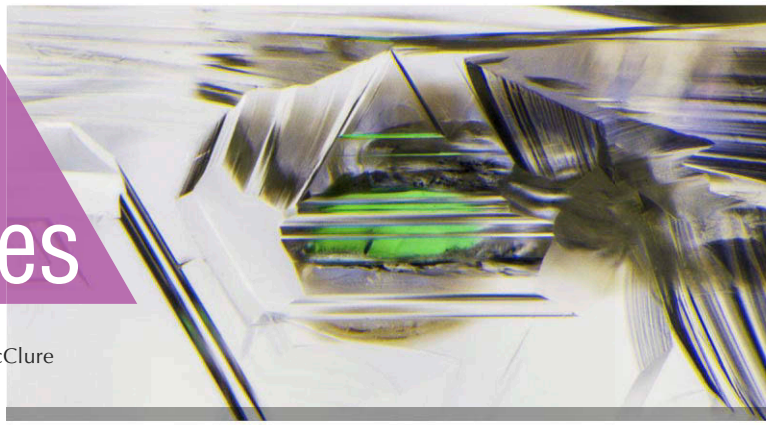

## Cat's-Eye ANDRADITE

The Carlsbad laboratory received a 49.65 ct semitranslucent to opaque brownish yellow oval cabochon (figure 1) for identification. The stone's most notable feature was its display of cat's-eye phenomenon across the dome. It had a refractive index over the limit of the refractometer and a hydrostatic specific gravity of 3.74.

Raman spectroscopy was used to assist with the identification, and the data collected (figure 2) were matched with andradite garnet from the GIA reference database. Analysis by energy-dispersive X-ray fluorescence (EDXRF) showed a composition consistent with andradite garnet, $Ca_3Fe_2(SiO_4)_3$, further proof of the stone's identity.

Internally, the stone is host to very fine and tightly packed needle-like inclusions running parallel to the base. With the stone cut as an oval cabochon, light is reflected off the inclusions, creating a rolling eye across the dome. This phenomenon is common in many gemstone species, and the demantoid variety of andradite garnet has been known to display cat's-eye phenomenon (Spring 2018 Lab Notes, pp. 58–59). This stone is a larger example of cat's-eye andradite garnet.

*Nicole Ahline*

*Figure 1. A 49.65 ct brownish yellow andradite cabochon with chatoyancy across the dome.*

## Quench-Crackled Dyed Blue CHALCEDONY Resembling Larimar

Recently, GIA's Tokyo laboratory examined five round beads that were semitransparent to opaque and showed blue to greenish blue bodycolors with a network-like structure of whitish zones (figures 3 and 4). These beads were acquired at an ornamental gem material shop in Tokyo and were sold as "sea-blue chalcedony," but the resemblance to Larimar led to our investigation.

The beads were identified as chalcedony based on spot RI readings of 1.53 to 1.54, SG values ranging from 2.48 to 2.65, and microscopic features such as parallel curved bands (figure 4B). Raman spectroscopic features (figure 5) also suggested that the beads were mainly composed of quartz crystals and matched chalcedony (e.g., D. Pop et al., "Raman spectroscopy on gem-quality microcrystalline and

*Figure 2. Raman spectrum of the cat's-eye andradite compared to the known reference. Spectra are offset vertically for clarity.*

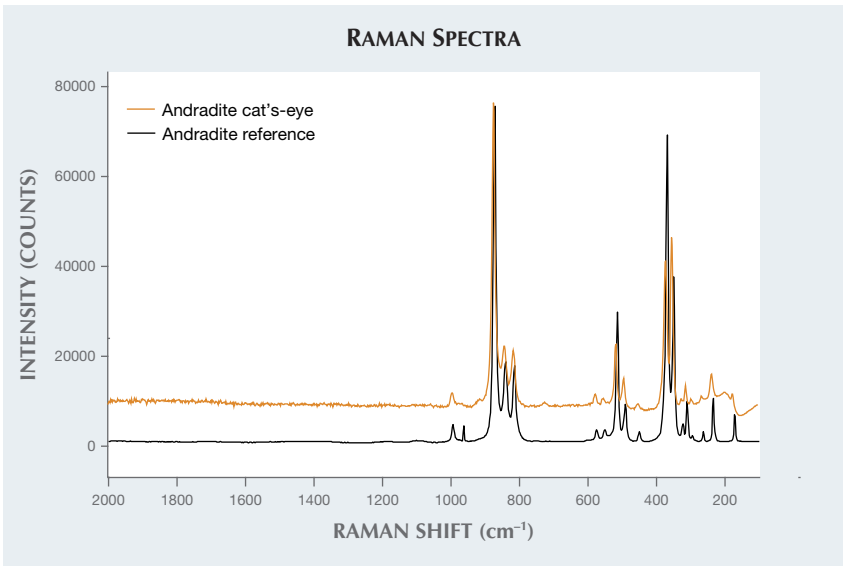


*Editors' note: All items were written by staff members of GIA laboratories.*

Gems & Gemology, Vol. 56, No. 2, pp. 281–291.

*Figure 3. Two of five round beads of quench-crackled dyed chalcedony and a pear-shaped Larimar cabochon. The bottom bead is 10.25 mm in diameter.*

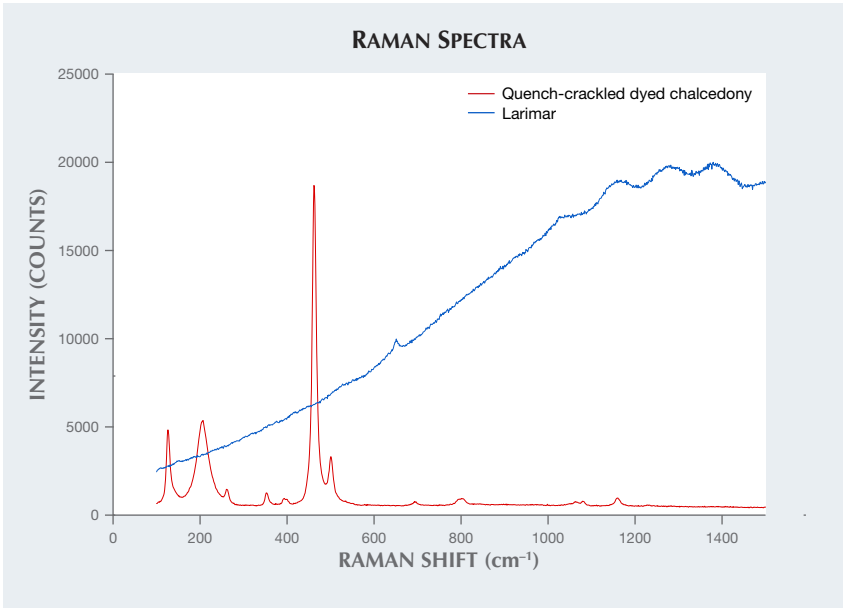


*Figure 5. Raman spectra of quench-crackled dyed blue chalcedony (red trace) and Larimar (blue trace). The dyed chalcedony Raman peaks match those of chalcedony and not Larimar.*

amorphous silica varieties from Romania," *Studia Universitatis Babeș-Bolyai, Geologia*, Vol. 49, 2004, pp. 41–52). Raman spectra of the beads showed no characteristics of chrysocolla (Spring 2020 Gem News International, pp. 188–189). Qualitative EDXRF analysis detected peaks related to Si, Fe, and Cu, indicating that Cu was likely the color-causing element. Ultraviolet-visible (UV-Vis) spectra also showed a broad band from 500 to 1000 nm that corresponded with Cu. There was no polymer detected by Fourier-transform infrared (FTIR) spectroscopy and no reaction when touched with a hot point. Under a gemological microscope, the stones revealed whitish zones following fractures. In order to consider the overall structure of such fractures, we cut them in half. Cross sections of the beads showed that the fractures with whitish zones were concentrated on the surface (figure 6). Such a structure is a known characteristic of quench-crackled dyed chalcedony and was reported previously (see Winter 2009 Lab Notes, p. 288). These beads probably represent a new color variety.

These quench-crackled dyed chalcedonies resemble Larimar in color and appearance. Larimar is a rare blue variety of pectolite with the ideal chemical formula of $NaCa_2Si_3O_8(OH)$ that displays white, green, and pale to sky blue colors. Blue color seen in Larimar is believed to be caused by the presence of small amounts of $Cu^{2+}$ within its structure (e.g., R.E. Woodruff and E. Fritsch, "Blue pectolite from the Dominican Republic,"

*Figure 6. Cross sections of two round beads of quench-crackled dyed chalcedony, 10.25 mm in diameter. Note that the white color is concentrated on the surface and along internal fractures.*

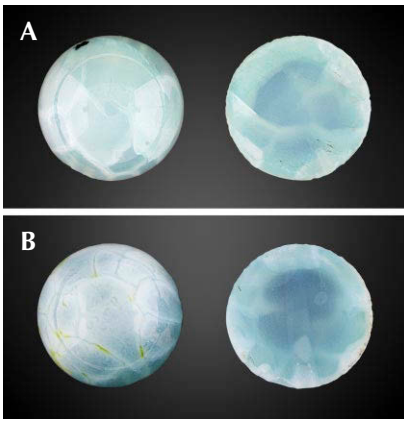


*Figure 4. A: A quench-crackled dyed chalcedony bead containing whitish zones following fractures; field of view 11.80 mm. B: Another bead showing a curved banding structure; field of view 12.80 mm. C: A pear-shaped Larimar cabochon (also shown in figure 3); field of view 16.20 mm. Note that it has a mottled blue and white color and contains other mineral inclusions.*

Winter 1989 *G&G*, pp. 216–225). We compared these beads with Larimar (the pear cabochon on the right in figure 3) to reveal their differences. The Larimar cabochon showed a mottled blue and white color with network-like whitish zones and other natural mineral inclusions (figure 4C) (again, see Woodruff and Fritsch, 1989). It had a spot RI reading of 1.60 and an SG of around 2.80. On the other hand, the quench-crackled dyed blue chalcedony beads had whitish zones following a network of fractures (figure 4B) and no other mineral inclusions.

This material can easily be separated from Larimar using standard gemological testing such as RI and SG. Advanced testing is useful in confirming the cause of blue color and the presence of polymer treatment.

*Makoto Miura*

## DIAMOND

### Irradiated Blue Diamond with Interesting DiamondView Image

We often receive lab-irradiated diamonds at the laboratory that have either natural or laboratory-grown origins (e.g., Summer 2018 Lab Notes, pp. 215–216). However, we recently received a 1.00 ct Fancy Deep greenish blue irradiated diamond (figure 7) with some unusual gemological features. The diamond's spectra and imaging showed that it had received artificial irradiation likely followed by annealing, which created unusually high concentrations of nitrogen vacancy (NV) centers.

As with most lab-irradiated diamonds, it was irradiated with the table side down; thus, the culet facing the beam received the highest dose of irradiation while much of the table facet was comparatively protected. The irradiated pavilion shows orange fluorescence due to a high concentration of NV centers (figure 8, left). Irradiated diamonds are often subjected to some low-temperature annealing after irradiation in order to "stabilize" the defects (e.g., Spring 2018 Gem News International, pp. 105–107); however, we generally do not see evidence of NV centers forming from that low-temperature heating.

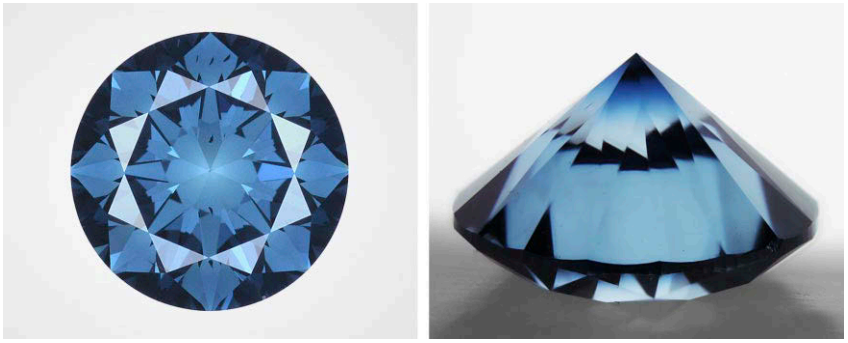

*Figure 7. This 1.00 ct Fancy Deep greenish blue diamond (left) owes its color to artificial irradiation, which is also evidenced by the color concentration at the culet (right).*

Here we see a combination of treatment conditions that generated an NV-related fluorescence on the pavilion and the crown; however, the original blue fluorescence of the natural, pre-irradiated diamond persists on the table, which was "shielded" during the irradiation (figure 8, right). The table experienced a lower radiation dose, fewer NV centers formed as a result, and we observe a transition from the orange NV fluorescence to the intrinsic blue fluorescence. Thus, the DiamondView fluorescence collected from the table creates an intriguing image.

The combination of the intrinsic defect concentrations along with the specific irradiation dose and subsequent annealing conditions created an unusual treated diamond for scientific study and an interesting reinterpretation of a "nailhead" diamond—a term often applied to a poorly cut stone that is dark on the table. Here, this effect can only be revealed under UV illumination.

*Sally Eaton-Magaña*

### Multiple Radiation Stains Suggest Interesting Geological Residency

A rough diamond crystal weighing 4.05 ct was observed with radiation staining on its surface. Radiation staining is thought to occur when radioactive fluids or minerals are adjacent to a diamond crystal in the earth. The radiation imparts damage to the

*Figure 8. The DiamondView fluorescence images of the irradiated diamond collected from the pavilion (left) show a high concentration of NV centers creating the orange fluorescence. On the table (right), the NV concentration has decreased sufficiently so that the NV-related orange fluorescence transitions to the diamond's intrinsic blue fluorescence.*

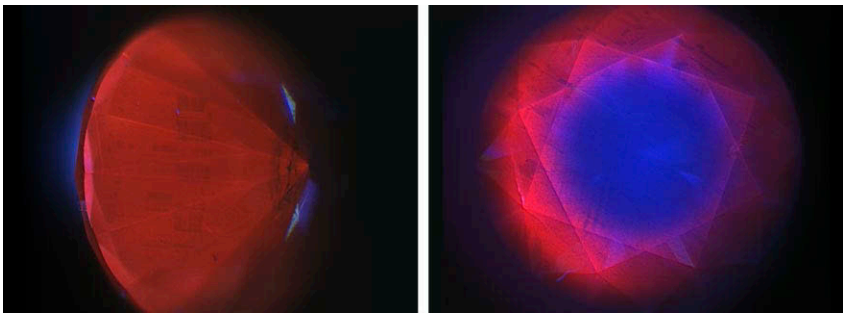

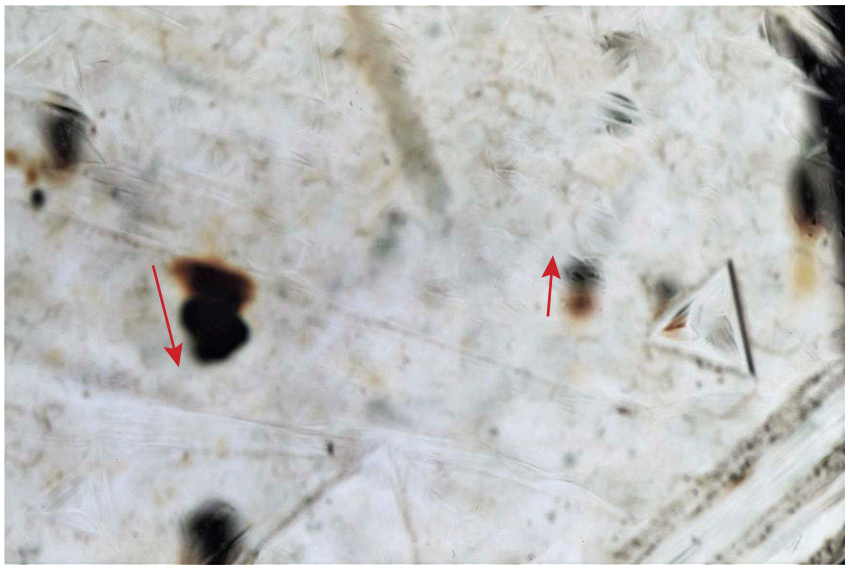

*Figure 9. Radiation staining is visible on opposite sides of the rough diamond crystal. On the upper surface the green stain is closer to the bottom of the image, whereas on the lower surface the green stain is closer to the top of the image. The arrows indicate the direction of displacement, which are in opposite directions on opposite sides of the rough crystal. Field of view 2 mm.*

diamond lattice, leaving behind vacancies and interstitial carbon atoms. When initially formed, these stains are green or greenish in color. If they are subjected to heat, the stains will turn to a brownish color. This particular diamond had both green and brown radiation stains on the surface. Nearly all of the stains existed in pairs, one brown and one green, and were of the same shape. This has been reported previously (C.M. Breeding et al., "Natural-color green diamonds: A beautiful conundrum," Spring 2018 *G&G*, pp. 2–27), and the proposed mechanism is that the diamond crystal is adjacent to a radioactive substance that imparts a green stain. When the diamond crystal is shifted slightly, the radioactive minerals create a new stain of the same shape but slightly displaced. The diamond was heated before the second set of stains had formed, which turned the initial set of stains brown.

In this rough crystal, the stain pairs are on opposite sides and in opposite directions (figure 9). The shift must have occurred in the direction from brown to green, which means this crystal most likely rotated with respect to its environment. The other explanation is that the host material on either side shifted in opposite directions by roughly the same amount.

To examine the spectroscopic differences between the green and brown radiation stains, we collected photoluminescence (PL) maps using 532 and 455 nm excitation in confocal mode. We collected data on several of the radiation stains but will focus this discussion on three of them (figure 10). Figure 10A has dark, almost black coloration in the center with dark green and brown color around the periphery. Figure 10B shows green and brown radiation stains but with a colorless section between them, and figure 10C has very light radiation staining.

In the radiation stain imaged in figure 10A, the diamond Raman peak was quite broad and distorted within the radiation stain compared to the surrounding diamond (figure 11, inset). The broadened and distorted Raman peaks are indicators of the radiation damage brought upon these areas and are consistent with prior observations of other very dark radiation stains (e.g., S. Eaton-Magaña and K.S.

*Figure 10. A portion of one side of the 4.05 ct rough diamond (left; field of view 3 mm) shows the relative placement of several radiation stains that are detailed with PL mapping at right. A: The photographed image of a very dark radiation stain and the corresponding PL map of diamond Raman intensity. B: The image of a brown radiation stain separated from its green counterpart and the corresponding PL map of its diamond Raman intensity. C: An image of a light radiation stain. Its PL map plots the TR12 intensity, instead of Raman intensity as in A and B, which was much higher within the radiation stain than within the colorless section. The PL maps in A and B were collected with 532 nm excitation and plot the diamond Raman peak area at 573 nm, while the map in C with 455 nm excitation plots the TR12 peak area at 470 nm and normalized to the diamond Raman peak area.*

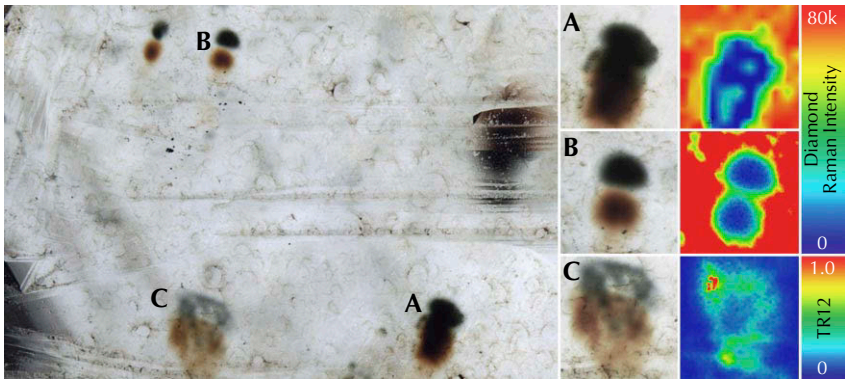

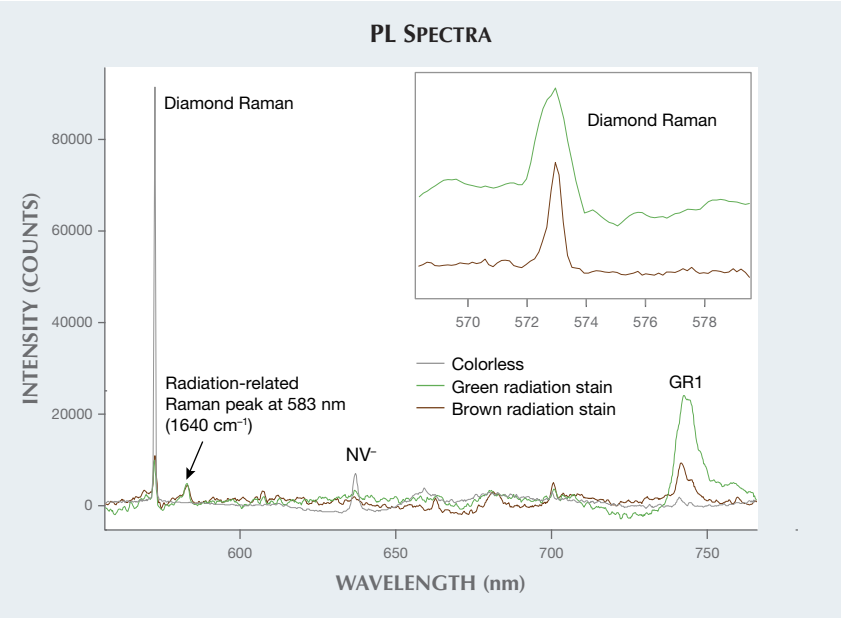


*Figure 11. These 532 nm excitation spectra show differences in features between the brown and green radiation stains imaged in figure 10A and a nearby colorless portion of the diamond. In the colorless diamond, the Raman peak is much larger and shows the $NV^-$ peak and a weak GR1. The brown and green stains show much lower diamond Raman intensity, and the peak width is greater within the green stain (inset). Both the green and brown radiation stains also show a radiation-related Raman peak at 1640 $cm^{-1}$ (583 nm; Eaton-Magaña and Moe, 2016) and comparatively pronounced GR1 peaks. Other unknown and intrinsic features are also present in these spectra.*

Moe, "Temperature effects on radiation stains in natural diamonds," *Diamond and Related Materials*, Vol. 64, 2016, pp. 130–142). The average Raman peak FWHM (full width at half maximum) within the green portion of the radiation stain was ~1.6 nm, while the average width within the brown portion of the radiation stain was ~1.1 nm. For comparison, the Raman width in the colorless sections was ~0.5 nm. The detected Raman intensity was also much lower than that of the surrounding colorless diamond (figures 10A and 11). Natural diamond and irradiation-related features such as TR12 (470 nm), H3 (503.2 nm), and $NV^-$ (637 nm) were not detected within this heavily damaged radiation stain. The GR1 peak was detected, though with higher intensity within the green radiation stain (figure 11).

In figure 10B, the PL map is consistent with the visual image and shows the area between the green and brown radiation stains approaching the features of the surrounding colorless diamond. Both figures 10B and 10C show indications of less radiation damage compared to figure 10A. The TR12, H3, and $NV^-$ features were detected in both the green and brown radiation stains, and the natural diamond features of H3 and $NV^-$ showed higher intensity in the brown. The GR1 and TR12 were slightly higher in the green radiation stains than in their brown counterparts and greater still than in the surrounding colorless diamond (figure 10C). For the radiation stains pictured in figures 10B and 10C, the diamond Raman widths were generally equivalent to those of the surrounding diamond. The PL maps also demonstrated that the boundary of the high GR1 intensity extended laterally ~30 µm beyond the colored radiation stain and into the surrounding colorless diamond; this is consistent with prior estimates of alpha radiation penetration (Eaton-Magaña and Moe, 2016).

In the radiation stains shown in figure 10, the brown portions of the radiation stains displayed features closer to the intrinsic diamond (lower diamond Raman width of the radiation stain shown in figure 10A and its corresponding spectra shown in figure 11, along with higher intensities of H3 and $NV^-$ of radiations stains shown in figures 10B and 10C; spectra not shown). These features suggest that the time and temperature that created the transition from green to brown as the diamond shifted to a new position also brought some "healing" from the localized radiation effects detected within the green radiation stains. This sample was interesting scientifically, as it allowed some direct comparison of radiation stain features created by the same point sources.

*Troy Ardon and Sally Eaton-Magaña*

## HEMIMORPHITE Resembling Paraíba Tourmaline

A 5.61 ct semitransparent blue cabochon (figure 12) was submitted to the New York laboratory for a Paraíba tourmaline origin report because of its electric blue color and its similar RI and internal features. Microscopic observation revealed parallel tubes,

*Figure 12. This 5.61 ct electric blue cabochon was identified as hemimorphite.*

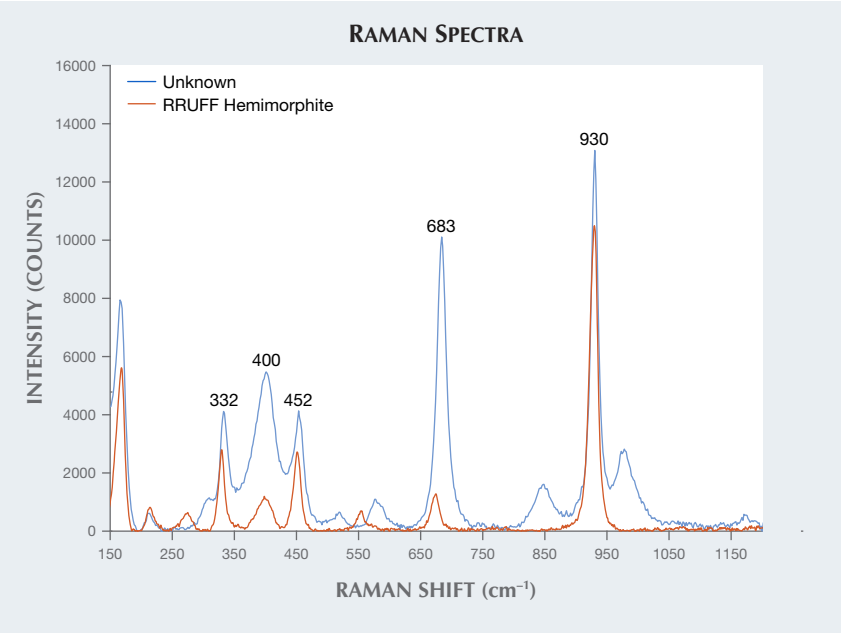


*Figure 13. Raman spectra of a 5.61 ct semitransparent blue cabochon that matched with hemimorphite in the RRUFF database (no. R070536).*

fluid inclusions, and white granular flake-like inclusions. The stone's optic character could not be determined due to the cabochon shape and abundance of inclusions, and only an approximate RI of 1.61–1.63 with a birefringence of 0.02 could be obtained. Specific gravity was 3.45, which is inconsistent with tourmaline, and the fluorescence reaction was medium blue under short-wave and inert under long-wave UV radiation. We confirmed its identity by Raman spectroscopy, which showed a match with hemimorphite (https://rruff.info/Hemimorphite/R070536), as shown in figure 13.

Hemimorphite is a zinc silicate, $Zn_4Si_2O_7(OH)_2 \cdot H_2O$; the purest form is white or colorless. Impurities cause different colors, such as copper ($Cu^{2+}$) for a bluish and greenish tint, ferrous iron ($Fe^{2+}$) for green, and ferric iron ($Fe^{3+}$) for brown. Laser ablation–inductively coupled plasma–mass spectrometry (LA-ICP-MS) composition analysis revealed that this stone contained no iron but did contain copper, which produced the electric blue color.

*Sudarat Saeseaw*

## SAPPHIRE

### Exceptional Purple Montana Sapphire

The Carlsbad laboratory recently received a 10.47 ct purple octagonal modified brilliant-cut sapphire (figure 14) for an identification and origin report. Standard gemological testing gave a 1.762 to 1.770 refractive index, indicating corundum, and a hydrostatic specific gravity (SG) of 4.00. The stone displayed no fluorescence under long-wave and short-wave UV.

*Figure 14. This 10.47 ct sapphire is notable as a large, unheated purple sapphire from Montana.*

Microscopic examination showed an interesting combination of inclusions, including an iridescent healed fissure surrounding a crystal, particulate clouds with intact and unaltered rutile needles/silk, flaky stringers, and twinning with intersection tubules

*Figure 15. Flaky particles and stringers of colorful rutile silk seen in the 10.47 ct purple Montana sapphire. Field of view 1.58 mm.*

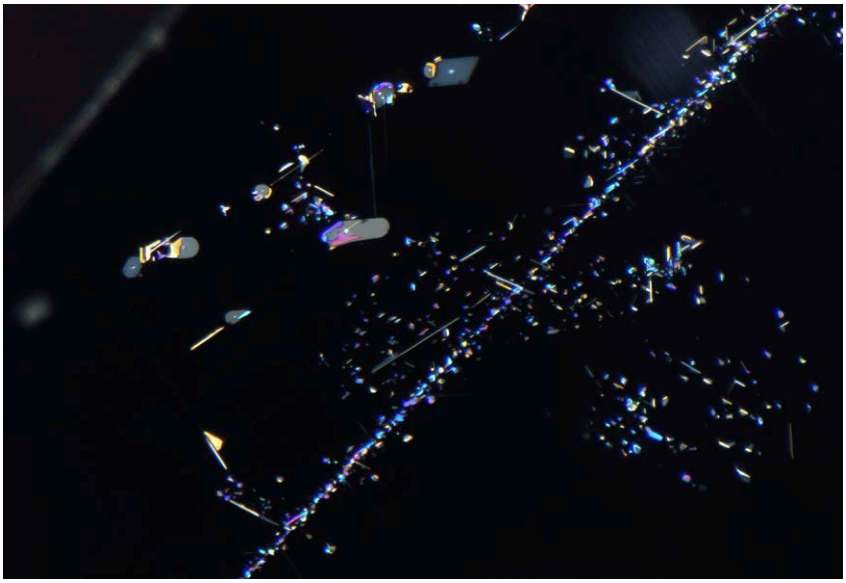

(figure 15). This inclusion scene is consistent with unheated corundum from Montana (Winter 2018 Lab Notes, pp. 434–435).

Laser ablation–inductively coupled plasma–mass spectrometry (LA-ICP-MS) was used to conclusively determine the stone's trace element chemistry, and the results were compared to corundum samples from GIA's colored stone reference collection. Trace element measurements indicated ranges of 13.6–15.0 ppma Mg, 13.1–15.0 ppma Ti, 7.76–8.36 ppma V, 38.3–39.4 ppma Cr, 1560–1600 ppma Fe, and 16.5–17.0 ppma Ga. The chemistry matched well with reference stones GIA has collected from Montana's secondary deposits. With a combination of microscopic observation, advanced testing, and GIA's reference collection, we were able to confirm the geographic origin of this sapphire.

Of all North American corundum localities, Montana reigns supreme. While rubies are only rarely found, facet-quality sapphire is mined at a number of different locations. Fine blue and purple gems have been mined at Yogo Gulch in central Montana, but cut gems over one carat are rare. Fancy sapphires are found associated with the placers of Missouri River and at Dry Cottonwood Creek and Rock Creek. These deposits produce larger material, but the colors tend to be pale. The successful development of heat treatment technology there has renewed interest in Montana sapphire.

This particular gem is consistent with those found in Montana's secondary deposits. It is a particularly fine example due to its saturated purple color, large size, and absence of heat treatment.

*Maryam Mastery Salimi and Nathan Renfro*

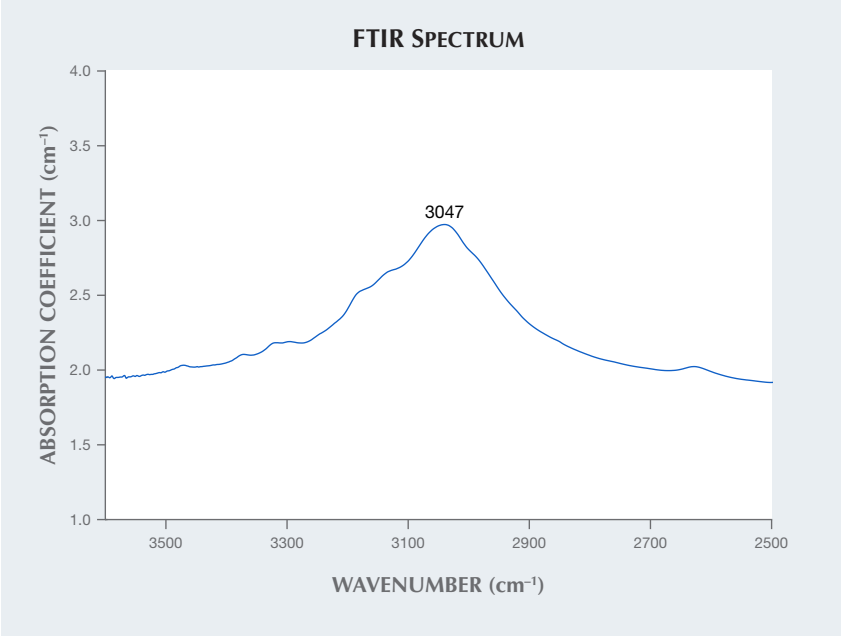


*Figure 16. The blue sapphire's FTIR spectrum shows a strong absorption band centered around 3047 cm⁻¹, suggesting treatment with heat and pressure.*

## Negative Crystal Containing a Mobile $CO_2$ Bubble in Blue Sapphire Heated with Pressure

Among the common inclusions seen in almost every mineral are primary cavities, or negative crystals. Negative crystals in sapphire are usually filled with liquid and gaseous carbon dioxide ($CO_2$) and may also contain solids such as diaspore or graphite.

At GIA's Bangkok laboratory, the author recently examined a 6.41 ct transparent blue faceted sapphire. It had a refractive index of 1.760–1.768, and its fluorescence reaction was inert under long- and short-wave UV radiation. Fourier-transform infrared (FTIR) spectroscopy is a useful technique to determine heat treatment in corundum. The sample's FTIR spectrum (figure 16) showed a broad band centered around 3047 cm$^{-1}$ that has been reported in sapphires treated with heat and pressure (M.S. Krzemnicki et al., "Sapphires heated with pressure – A research update," Spring 2019 *InColor*, pp. 86–90).

Microscopic observation revealed altered growth tubes, dissolved particles, melted crystals with altered fingerprints, and small birefringent crystals in a low-relief partially healed fissure (figure 17), proof of high-temperature heat treatment with pressure (Winter 2018 Gem News International, p. 458). When the sapphire was gently heated by the microscope bulb, the gas bubble became smaller and disappeared as the gas and liquid homogenized. The presence of $CO_2$ fluid inclusions in negative crystals is important evidence of natural origin and the absence of thermal enhancement (J.I. Koivula, "Carbon dioxide fluid inclusions as proof of natural-colored corundum," Fall 1986 *G&G*, pp. 152–155). Interestingly, this sample exhibited a rounded bubble in a negative

*Figure 17. When the sapphire was viewed under cross-polarized light, a plane of small birefringent crystals was observed in a partially healed fissure. Field of view 4.10 mm.*

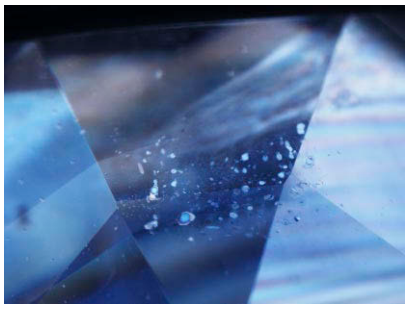

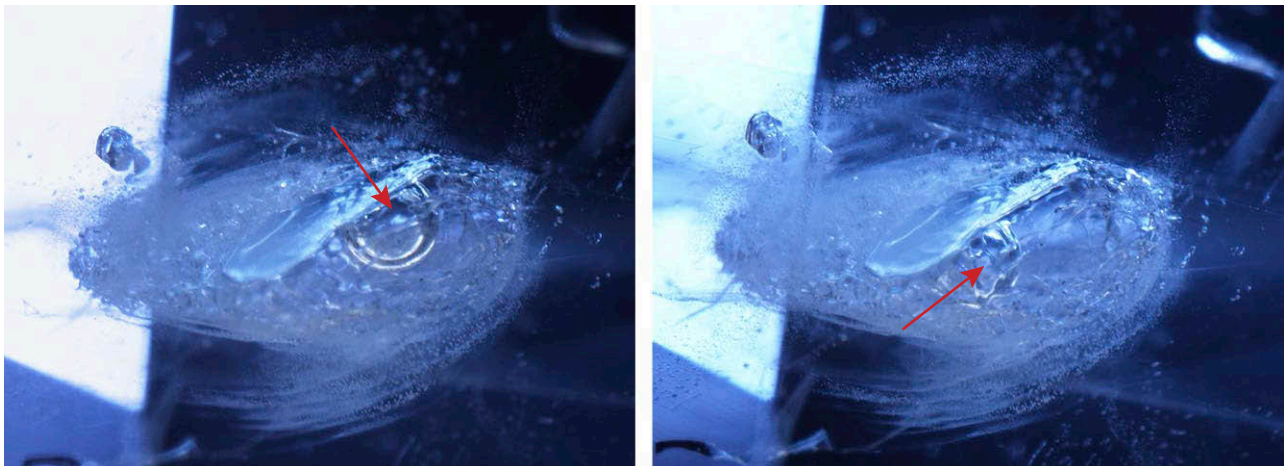

*Figure 18. A negative crystal with a mobile $CO_2$ bubble in the blue sapphire heated with pressure. Field of view 2 mm.*

crystal that moved and was still observed when gently heated with a hot point (figure 18). Raman spectroscopy confirmed the bubble as carbon dioxide ($CO_2$). To our knowledge, a mobile $CO_2$ bubble in a negative crystal has not been reported in a sapphire heated with pressure.

*Nattida Ng-Pooresatien*

*Figure 19. An 11.16 ct pink sapphire from Mozambique.*

## Pink Mozambique Sapphire

Recently, GIA's Carlsbad lab received an 11.16 ct pink sapphire (figure 19) for a colored stone identification and origin report. Standard gemological testing was consistent with sapphire, giving a refractive index of 1.759–1.769 and a hydrostatic specific gravity of 4.00.

The sapphire contained various inclusions (figure 20) such as negative crystals and transparent colorless crystals. These inclusions showed no indication of thermal alteration, suggesting the stone was unheated. Bands of silk arranged in a hexagonal formation with irregularly shaped thin films intermixed with particle clouds could be seen throughout the stone. This suite of inclusions was consistent with a Mozambique origin.

Advanced testing confirmed that the sapphire was unheated and from Mozambique. Infrared spectroscopy produced a spectrum consistent with unheated sapphire. The spectra showed a single peak at 3309 $cm^{-1}$ with no secondary peak at 3232 $cm^{-1}$ (Summer 2019 Gem News International, pp. 290–291). Laser ablation–inductively coupled plasma–mass spectrometry (LA-ICP-MS) confirmed the stone's chemical composition of a higher iron and lower vanadium content, which is typical of Mozambique sapphires.

Mozambique is known for rubies that are saturated in color. With its 11.16 ct size and pure pink hue, this unheated Mozambique sapphire was a unique encounter.

*Nicole Ahline*

*Figure 20. A negative crystal (left; field of view 1.79 mm) and a cluster of silk (right; field of view 2.57 mm) that could be seen throughout the pink sapphire.*

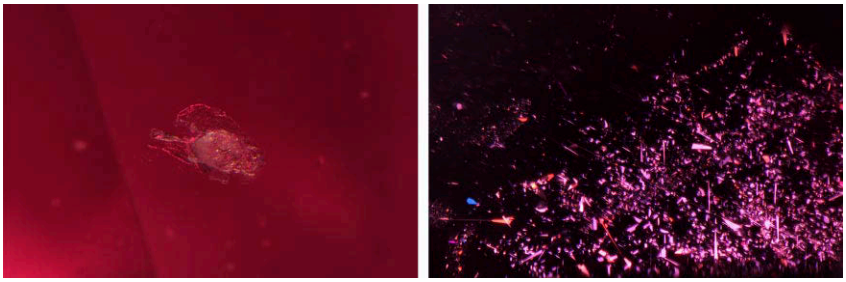

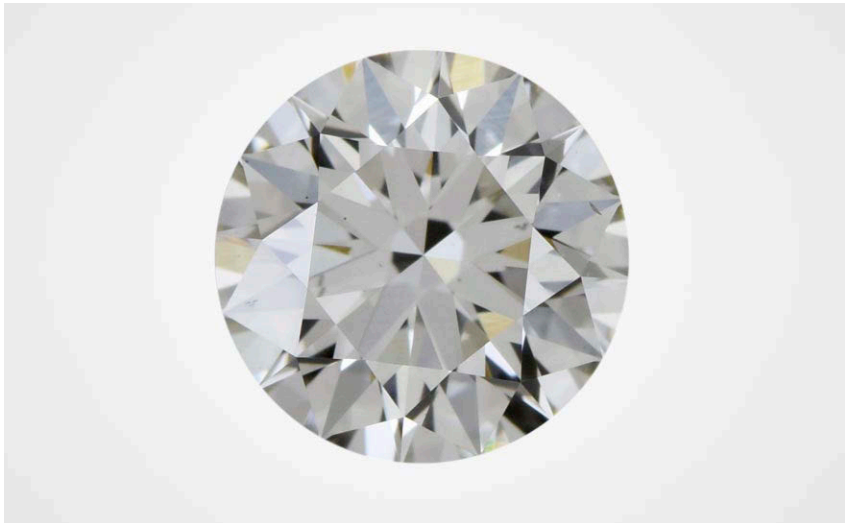

*Figure 21. Face-up image of one of the HPHT-processed CVD laboratory-grown diamonds submitted to the Antwerp lab. This 1.02 ct round brilliant synthetic diamond has J-equivalent color and $VS_2$ clarity.*

## SYNTHETIC DIAMOND

### HPHT-Processed CVD Laboratory-Grown Diamonds with Low Color Grades

When CVD-produced diamonds are grown with nitrogen added to the gas mixture, or when the growth rate is relatively high, the as-grown crystal ends up having an undesirable brown color. In order to improve this color, CVD-grown diamonds are often treated at high-pressure, high-temperature (HPHT) conditions after their growth. The Antwerp laboratory recently received 11 CVD laboratory-grown diamonds that had been subjected to HPHT treatment after growth but still had a relatively uniform low color grade (J-equivalent, figure 21).

The samples were round brilliants with weights ranging from 1.02 ct to 1.33 ct and clarity grades in the VS range. Commonly observed clarity characteristics were crystals, needles, and pinpoints along with feathers. They were classified as type IIa diamonds with weak additional absorption peaks at 1332, 1344, 2947, and 3031 $cm^{-1}$. Four showed a weak absorption peak at 3107 $cm^{-1}$ (N3VH). None of them showed the CVD-specific $NVH^0$ band at 3123 $cm^{-1}$ (P.M. Martineau et al., "Identification of synthetic diamond grown using chemical vapor deposition [CVD]," Spring 2004 *G&G*, pp. 2–25). UV-visible absorption spectra taken at liquid nitrogen temperature revealed the presence of the $SiV^-$ center, a defect commonly observed in CVD synthetic diamonds. Photoluminescence (PL) spectra taken with various excitation wavelengths and at liquid nitrogen temperature showed the presence of a strong $SiV^-$ doublet (736.6/736.9 nm), strong $NV^{0/-}$ (575 and 637 nm) centers, numerous peaks in the 520–550 nm region, and a strong H3 (503.2 nm) center. Furthermore, all the spectra showed an absence of the $SiV^0$ (946 nm) and 596/597 nm centers. This last center is commonly observed in as-grown CVD synthetic diamonds but is removed by post-growth HPHT treatment. A weak H2 center (986 nm) was observed in six stones. Weak Ni-related absorption peaks were detected in 830 nm PL spectra of all the samples, but at higher wavelengths than expected (884–885 nm, potentially attributed to high strain). Microscopic analysis using crossed polarizing plates confirmed the presence of strain throughout the stones.

*Figure 22. DiamondView image of one of the 11 CVD samples shows green fluorescence and clear linear growth striations. The layers indicate stop-start growth.*

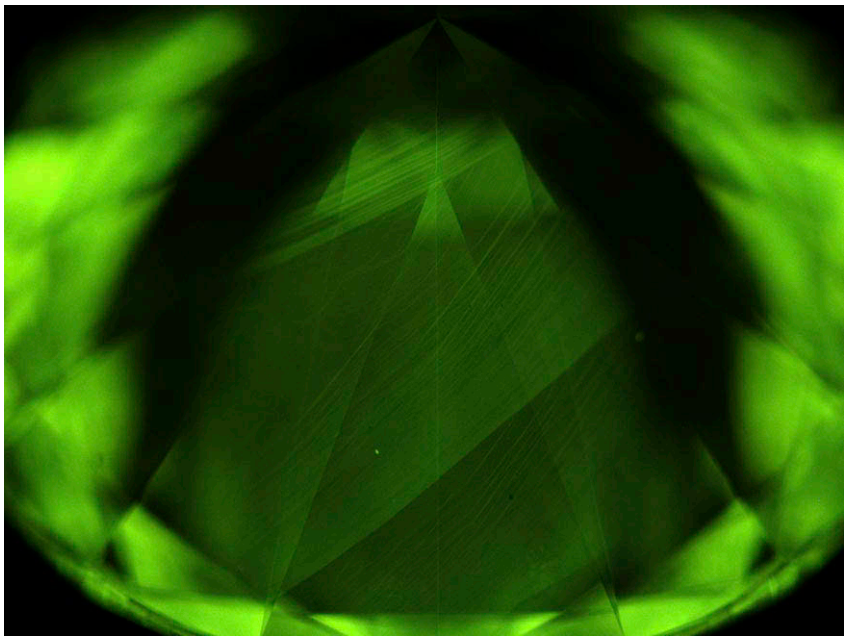

*Figure 23. This 3.02 ct HPHT-grown diamond with color equivalent to Fancy Vivid pink had an unstable color.*

DiamondView images showed green luminescence (linked to the strong H3 center revealed by PL spectra) and a weak bluish green phosphorescence. All samples showed clear linear growth striations. Some revealed a multilayer stop-start growth. The orientation of the growth layers gives an indication of the angle at which the stone is cut from the rough plate (figure 22).

Based on all the observations, we conclude that the analyzed CVD laboratory-grown diamonds underwent HPHT treatment after growth. Their relatively low color grades are believed to be linked to the duration of the treatment. More efficient treatment would likely result in a higher color grade.

*Ellen Barrie*

## HPHT Laboratory-Grown Pink Diamond with Unstable Color

While rare, it is not uncommon for certain types of diamond to change color when exposed to different lighting or thermal conditions. Consider, for example, chameleon-type diamonds, which can change color from yellowish green to orangy yellow when heated or concealed in the dark for long periods of time.

*Figure 24. Left: Strong color zoning observed under natural lighting conditions. Right: The fluorescence pattern follows this zoning, as observed in the DiamondView image (strong short-wave UV).*

Recently submitted to GIA's New York laboratory for examination was a 3.02 ct laboratory-grown diamond with the equivalent color grade of Fancy Vivid pink (figure 23). Typical of an HPHT-grown laboratory-grown diamond, it exhibited strong color zoning (figure 24, left) related to its typical hourglass synthetic growth structure. Of note, it exhibited very strong orange fluorescence when exposed to ultra-short-wave ultraviolet radiation (figure 24, right). This is of note as it is indicative of post-growth treatment to create the desirable pink color.

This diamond was grown with a very carefully controlled nitrogen content that produced approximately 1.6 ppm of type Ib single substituted nitrogen (post treatment). The nitrogen content was calculated from a normalized mid-infrared spectrum. Post-growth treatment of irradiation/annealing generated very strong absorption from the nitrogen vacancy (NV) centers that are responsible for both the pink bodycolor and the very strong orange-red fluorescence (see the PL spectrum in figure 25).

*Figure 25. 514 nm (green) photoluminescence spectrum showing strong NV (nitrogen vacancy) centers at 575 and 637 nm. These are responsible for the very strong bodycolor and orange-red fluorescence.*

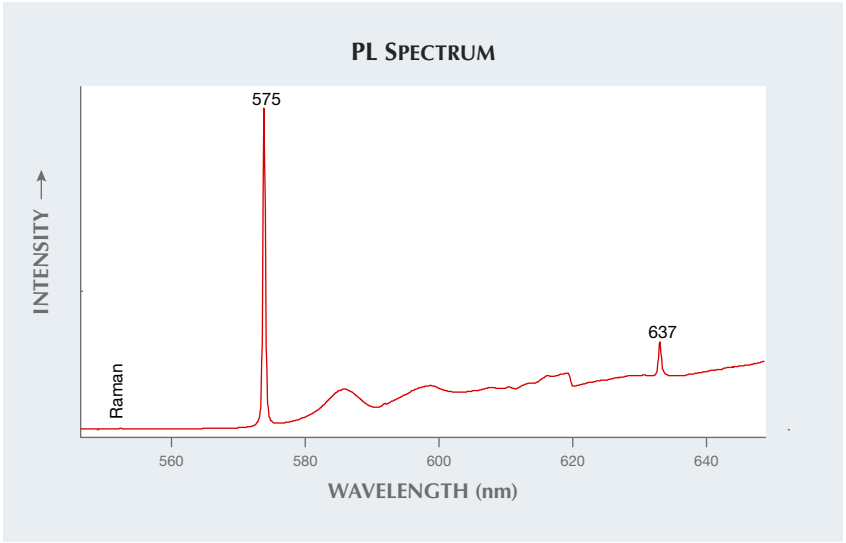

*Figure 26. A dramatic hue shift from pink to orange was observed when the synthetic diamond was exposed to short-wave UV radiation. Color swatches (bottom) were generated from recorded LCH values both before and after UV bleaching. The two images (top) were taken using standard lighting in the GIA colorimeter, which recorded the LCH values.*

When excited by short-wave UV radiation, the nitrogen vacancy color-causing centers are bleached and desaturated, resulting in a hue shift to orange (figure 26). This is a temporary color change, and within minutes the diamond will revert to its stable pink color under normal daylight conditions.

Using LCH (lightness, chroma, and hue) values, color swatches (figure 26, bottom) were generated that accurately represent the color change observed. The images in figure 26 (top) were captured using a GIA-built colorimeter with standard lighting conditions.

With the recent influx of laboratory-grown fancy-color diamond into the market, these phenomena are of note to consumers.

*Kaitlyn Mack and Paul Johnson*

*PHOTO CREDITS*
*Diego Sanchez—1, 7 (left), 14; Shunsuke Nagai—3, 6; Makoto Miura—4; Sally Eaton-Magaña—7 (right), 8, 10; Troy Ardon—9; Nuttapol Kitdee—12; Aaron Palke—15; Nattida Ng-Pooresatien—17, 18; Robison McMurtry—19; Nathan Renfro—20; Ellen Barrie—21; Michaela Harinová—22; Jian Xin (Jae) Liao—23; Paul Johnson—24 (right)*